PUBLICATIONS OF THE ASTRONOMICAL SOCIETY OF THE PACIFIC, **125**:1336–1347, 2013 November

CHIRON—A Fiber Fed Spectrometer for Precise Radial Velocities

ANDREI TOKOVININ,[1] DEBRA A. FISCHER,[2] MARCO BONATI,[1] MATTHEW J. GIGUERE,[2] PETER MOORE,[1]
CHRISTIAN SCHWAB,[2,3] JULIEN F. P. SPRONCK,[2] AND ANDREW SZYMKOWIAK[2]

Received 2013 June 17; accepted 2013 September 12; published 2013 October 16

ABSTRACT. The CHIRON optical high-resolution echelle spectrometer was commissioned at the 1.5 m telescope at CTIO in 2011. The instrument was designed for high throughput and stability, with the goal of monitoring radial velocities of bright stars with high precision and high cadence for the discovery of low-mass exoplanets. Spectral resolution of $R = 79\,000$ is attained when using a slicer with a total (including telescope and detector) efficiency of 6% or higher, while a resolution of $R = 136\,000$ is available for bright stars. A fixed spectral range of 415–880 nm is covered. The echelle grating is housed in a vacuum enclosure and the instrument temperature is stabilized to $\pm 0.2°$. Stable illumination is provided by an octagonal multimode fiber with excellent light-scrambling properties. An iodine cell is used for wavelength calibration. We describe the main optics, fiber feed, detector, exposure-meter, and other aspects of the instrument, as well as the observing procedure and data reduction.

Online material: color figures

1. INTRODUCTION

While increasingly large astronomical telescopes with complex instrumentation are now being constructed, small and medium-size telescopes are still valuable, particularly for dedicated time-domain projects. Monitoring radial velocities (RVs) of stars for the discovery and characterization of exoplanets, binary companions, or pulsations are a few examples of projects that can be carried out with moderate aperture telescopes equipped with stable high-resolution optical spectrographs. Recently, several echelle spectrometers have been built and put into operation, e.g., SOPHIE (Perruchot et al. 2008), HERMES (Raskin et al. 2011), and PFS (Crane et al. 2010). This paper describes the CHIRON optical echelle spectrometer at the 1.5-m telescope in Chile (Schwab et al. 2010, 2012).

The 1.5-m telescope at Cerro Tololo Interamerican Observatory (CTIO) is operated by the SMARTS (Small and Moderate Aperture Research Telescope System) consortium where observing time is purchased by members. In addition, 25% of the time is distributed in an open competition by National Optical Astronomy Observatory (NOAO) and 10% is available to Chilean astronomers. The observations are done in service mode by telescope operators. This is an ideal arrangement for high-cadence observing programs and long-term RV monitoring. Unfortunately, the 1.5-m is too old for a cost effective conversion into a robotic facility.

In the 1980s, the *Bench Mounted Echelle* (BME) was developed for the 1.5-m telescope, and light was coupled to the instrument through a fiber (Barden & Ingerson 1998). This instrument was decommissioned in 2001, and after the retirement of the echelle at the Blanco 4-m telescope in 2004, the observatory was left without a high-resolution spectrograph, while FEROS and HARPS were intensively used at ESO, and the Du Pont echelle was used at Las Campanas. In 2008, a new fiber feed for the CTIO 1.5-m was constructed and adapted to the old Blanco Echelle. This combination, called the *Fiber Echelle*, was offered to SMARTS and NOAO users from 2008 to 2010 (e.g., Richardson et al. 2011), until it was replaced by CHIRON.[4]

The design for CHIRON was primarily driven by the need to measure RVs with high precision for searches for low-mass planets around nearby bright stars such as α Cen (Guedes et al. 2008). Our funding envelope (~600 K) did not allow us to put the entire instrument in a vacuum enclosure (in which case a thorium-argon wavelength calibration could be used), so an iodine cell was used for wavelength calibration. Iodine cells are often used with traditional slit spectrographs and yield high RV precision even for instruments without environmental stabilization (e.g., Fischer et al. 2012) because the iodine spectrum is embedded in the stellar spectrum and follows the same optical path through the instrument.

We considered design trade offs between high spectral resolution and the signal-to-noise ratio (S/N) that can be reached with a 1.5-m telescope. An important consideration is that

[1] Cerro Tololo Inter-American Observatory, Casilla 603, La Serena, Chile atokovinin@ctio.noao.edu.
[2] Department of Astronomy, Yale University, New Haven, CT 06511.
[3] Sagan Fellow.

[4] NSF ARRA MRI grant 0923441.

we limit the maximum exposure time for precise Doppler measurements to 15 minutes in order to limit errors in our barycentric correction. Even if nightly velocities are binned to increase the effective S/N, we model the Doppler shift in each observation individually and a S/N of at least 50 is needed to minimize errors in our model of the spectral line spread function (SLSF). The SLSF is sometimes called the point spread function (PSF); however, this is not an accurate term to use when referring to the instrumental smearing of spectral lines.

To set the top level requirement for resolution, we carried out simulations of photon-limited Doppler precision and found that a S/N of 200 and resolution of $R = 80\,000$ yielded internal errors of $1.2\ \mathrm{m\,s^{-1}}$. Increasing the simulated resolution to 120 000 improved the single measurement precision in our simulations for S/N of 200 to $1.0\ \mathrm{m\,s^{-1}}$ (see also Bouchy et al. 2001) However, the increased spectral resolution then required exposure times longer than 15 minutes in order to reach a S/N of 50 for the typical star on our program. Thus, we optimized the instrumental resolution for Doppler precision, with the desired S/N as limiting consideration.

A high premium was placed on the instrument stability, especially on stability in the SLSF (Spronck et al. 2013, 2012a, 2012b), so some thermal control was included and light was coupled to the instrument with a fiber. CHIRON is one of the few fiber-fed spectrometers using an iodine cell. Finally, we wanted to reach the highest possible efficiency to offset the small telescope diameter. With a fixed spectral format, CHIRON covers a broad spectral range and is useful for a wide variety of science programs. We made use of the existing acquisition/calibration/guiding module deployed in 2008 for the fiber echelle.

The instrument concept was developed in 2009. Its design and construction were completed in 1 year and science observations with CHIRON began in 2011 March. During the first year of operation, the internal RV measurement precision was about $0.8\ \mathrm{m\,s^{-1}}$, but the velocity rms scatter for chromospherically stable stars was generally about $2\ \mathrm{m\,s^{-1}}$. To further improve the RV precision, throughput, and stability, the instrument was upgraded between 2012 January and May in several respects. The old echelle grating was replaced by a new higher efficiency R2 Richardson grating mounted in a vacuum enclosure. We developed a sol-gel coating facility to apply an antireflective coating to some optics (the prism, echelle vacuum enclosure window, and other optics). We improved thermal control; an exposure meter for photon-weighted exposure timing was installed. The CCD controller was replaced, and the input fiber was changed from a circular to an octagonal fiber for better modal scrambling of the light.

The instrument is described in § 2. In § 3, the observing procedure and data reduction are briefly covered, while actual instrument performance is discussed in § 4. The paper closes with conclusions in § 5. Additional technical information on the instrument can be found on its web site.[5]

2. INSTRUMENT DESCRIPTION

CHIRON is located in the Coudé room of the 1.5-m telescope. It receives the light from a star (or a calibration lamp) through a multi-mode fiber, which is permanently installed at the telescope. The optical configuration and spectral format of CHIRON are fixed, covering the wavelength range from 415 to 880 nm in a single exposure (Fig. 1). The fiber image can be transformed by a slicer or masks, offering some flexibility. In the nominal mode with slicer, CHIRON reaches spectral resolution of $R = 79\,000$ with 3-pixel sampling. Each CCD pixel corresponds to $1.075\ \mathrm{km\,s^{-1}}$ in RV. For readers' convenience the main characteristics of the instrument are summarized in Table 1; they are discussed further in the paper.

2.1. Optical Design

Most modern high-resolution echelle spectrometers belong to two families. One of these is the double-pass Littrow design as, e.g., in SOPHIE (Perruchot et al. 2008) or PFS (Crane et al. 2010). Another is the white-pupil design pioneered by ELODIE (Baranne et al. 1996) and used in FEROS (Stahl et al. 1999), HARPS (Pepe et al. 2000), HERMES (Raskin et al. 2011), and other instruments. CHIRON has a pseudo-Littrow design; the beams before and after the echelle grating are separated by a relatively large angle of $2\gamma = 11°$ and go through different optics, resembling in this respect HERCULES (Hearnshaw et al. 2002), the Blanco Echelle, and some other classical spectrographs. This choice is driven by the simplicity and the desire to minimize the number of optical elements, boosting the efficiency; the loss of diffraction efficiency is only $\cos\gamma = 0.995$ (Schroeder & Hilliard 1980). A Littrow design with double pass through refractive optics and prism would have twice the chromatic aberration and a variable slit tilt along the orders.

The drawbacks of using an incidence angle $\gamma = 5.5°$ in the cross-dispersion direction are the elliptical beam footprint on the camera and the rotation of the slit image by 24°. This is compensated by appropriate counter-rotation of the entrance slit, at a cost of $\cos 24° = 0.91$ loss in resolution.

The light beam emerging from the fiber is transformed by small lenses and collimated by the 150-mm $F/4$ on-axis parabolic mirror before reaching the echelle grating (Fig. 2). The nominal beam diameter on the collimator is 130 mm. We used an old large R2 echelle during the first year after commissioning. However, this grating had a measured peak efficiency of about 55%. This grating was replaced during the CHIRON upgrade with a more efficient grating with a protected silver

[5] Please see http://www.ctio.noao.edu/noao/content/chiron for more information.

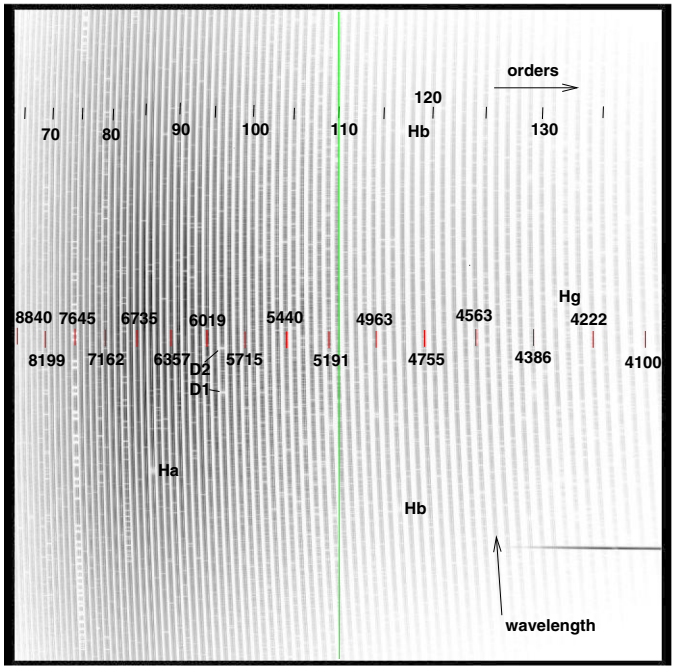

FIG. 1.—Order map of CHIRON. The order numbers are indicated on the *top*; central wavelengths of some orders and several characteristic lines are overlayed on the low-contrast negative display of the α Cen A spectrum. See the electronic edition of the *PASP* for a color version of this figure.

coating.[6] The new grating was procured from Richardson Labs/Newport: 31.6 lines/mm, nominal blaze angle 63.9°, Zerodur substrate of $135 \times 265 \times 45$ mm. The ruled area is 130×260 mm. The measured efficiency at blaze peak at $\lambda = 514$ nm is 82%. The 130-mm beam is slightly vignetted by the grating.

The new echelle grating is housed in a vacuum enclosure to significantly reduce variability in the temperature or pressure of the air layer in contact with the grating that would otherwise introduce changes in the dispersion. Light passes twice through the enclosure window, made of BK7 glass with a 1.5° wedge to avoid reflections. Nominal surface quality of the window is $\lambda/4$ with <4 fringes power. Reflection losses at window surfaces are minimized by the sol-gel anti-reflection (AR) coating on the window ($R < 0.25\%$ per surface at 500 nm). The reflectivity of the sol-gel coating increases to 2% at the blue and red ends of the CHIRON wavelength range. Double reflection from the window produces a bright feature in the blue part of the spectrum which is mostly outside the free spectral range. The vacuum echelle enclosure has 20-mm thick walls to minimize its mechanical reaction to changing atmospheric pressure.

The cross-dispersion prism was made out of a Schott LF7 glass blank by the TORC company in Tucson. This glass

[6] Please see http://gratings.newport.com/information/techdata/Coating_Reflectivity.pdf for more information.

TABLE 1

MAIN PARAMETERS OF CHIRON

$R = \lambda/\Delta\lambda$: 27 400, 79 000, 95 000, 136 000
Wavelength coverage: 415–880 nm
Spectral orders: 138 to 66
Collimator: $F = 600$ mm, beam diameter 130 mm
Grating: 63.9° blaze, 31.6 l/mm, 130×260 mm
Cross-disperser: LF7 prism, apex 62°, one pass
Camera: oil triplet $F = 1012$ mm, $D = 140$ mm
CCD: $4096(\mathrm{H}) \times 4112(\mathrm{V})$, 15 μm pixels, graded-AR
Fiber feed: 100 μm octagonal core, 2.7″ on the sky

was selected as a compromise between cost, availability, and uniformity of inter-order spacing. The prism apex angle is 62°, side length 260 mm, height 160 mm. Only one pass through the prism located *after* the echelle grating ensures a constant slit tilt along the orders; this is an advantage over the Littrow design with a prism in double pass. Inhomogeneity of the refractive index produces some aberration of the transmitted beam, despite an attempt to correct them by manual retouching of the prism. During the upgrade, the prism was sol-gel coated to optimize transmission at 500 nm and at 54° incidence angle (reflection loss at each surface $R < 0.6\%$ at 550 nm, $<2.5\%$ over entire wavelength range). The internal glass transmission averaged over the beam is 98%.

The camera is a commercial triplet lens APO-140 produced by Telescope Engineering Company.[7] This oil-spaced triplet lens has a light diameter of 140 mm. The focal length with a 2-element field flattener is 1012 mm. The manufacturer kindly provided the optical prescription, allowing us to evaluate the lens performance. The spot diagrams fit within 50 μm over the whole 60×60 mm square field (Fig. 3). The major residual aberration is chromatic defocus, so the lens is diffraction-limited at any given wavelength. The triplet and flattener lenses have broad-band AR coatings, with a typical loss of 0.25% per surface. The beam after the camera is folded by a 150-mm flat mirror custom-coated to 97% reflectivity, making the instrument more compact.

The wavelength range of CHIRON avoids the near-UV region (e.g., calcium H and K lines) because it would require a different custom-designed camera lens and because the fiber transmission degrades in the blue. As the iodine lines are concentrated in the 500–600 nm region of the spectrum, the loss of UV does not compromise the main goal of the instrument.

2.2. Image Slicer

Achieving high spectral resolution with a single fiber is possible by decreasing the fiber diameter (with associated light loss at input), increasing the beam size (and increasing the

[7] Please see http://www.telescopengineering.com for more information.

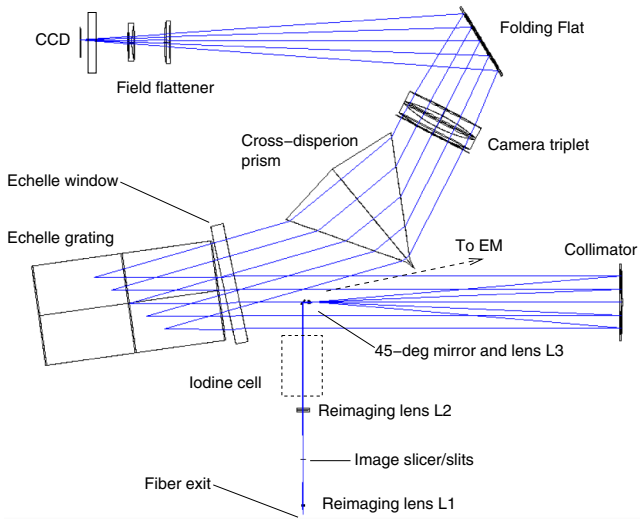

FIG. 2.—Layout of the CHIRON optics (*see text*). See the electronic edition of the *PASP* for a color version of this figure.

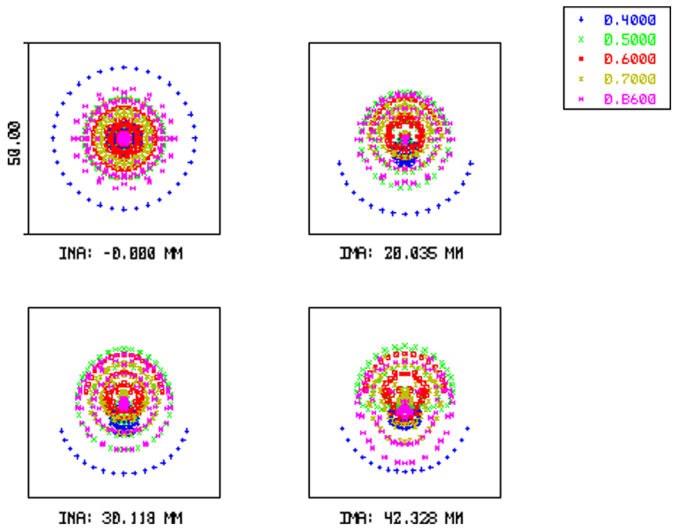

FIG. 3.—Spot diagrams of the APO-140 triplet in single pass. The size of each square is 50 μm. See the electronic edition of the *PASP* for a color version of this figure.

instrument cost), or using an R4 echelle (more orders on the detector). We have chosen to slice the fiber image in three segments, gaining a factor of 3 in resolution over the bare fiber without much light loss. CHIRON uses a Bowen-Walraven image slicer. For fabrication reasons, two mirrors replace the standard design with total internal reflection as used, e.g., in FEROS (Stahl et al. 1999). Mirrors with high reflectivity and sharp edges are available at low cost. As the three slices have 0, 2, and 4 reflections, respectively, the light loss is acceptably small (measured efficiency 0.82). The slicer is described in more detail by Schwab et al. (2010, 2012).

To reduce the defocus inherent to this image slicer, the $F/5$ beam emerging from the fiber is transformed to a slow $F/41$ ratio by a small lens L1 (Fig. 2). The fiber image is magnified 8.3 times, to 0.825 mm diameter; the sliced "slit" image is 0.27×2.4 mm. After the slicer, a second lens L2 of 100 mm focal length collimates the beam and, at the same time, forms the pupil image close to the following elements: the tiny diagonal mirror and a $F = 12.5$ mm lens L3 that couples the beam to the collimator. These elements are located near the collimator focus and supported by two thin vanes.

The reflective slicer is tunable and offers extra flexibility. By moving it out of the beam, the unsliced fiber image is passed into the instrument. The spectral resolution is thus degraded to $R = 27\,400$, but the fiber projects to a smaller number of binned pixels on the detector, increasing the S/N for faint stars. The slicer unit also holds two slit masks of 0.2 mm and 0.1 mm width that can block the fiber image by the same translation motion of the slicer unit. The wider slit provides similar resolution as the slicer, but with narrower and "cleaner" orders in the cross-dispersion direction. The narrow slit brings the resolution to $R = 136\,000$ at the expense of even larger light loss. These two slit masks are intended for observing very bright stars with an aim of achieving the highest RV precision. The four slit modes are summarized in Table 2. The resolution is determined from the measured FWHM of the line-spread function, SLSF. The last column gives the efficiency of each mode relative to the bare fiber.

2.3. Iodine Cell

For precise RV work, the iodine cell is inserted in the narrow (3 mm diameter) collimated beam after the second lens L2, without causing defocus. The cell is a glass cylinder of 50 mm diameter and 100 mm length filled with iodine vapor. Its windows are AR-coated on the external surfaces. It is placed in a heated and insulated container and maintained at $+40$°C stabilized temperature to keep all iodine vaporized. Owing to the insulation, the 10-W heater working typically at half-power is sufficient to maintain a constant cell temperature.

It would be preferable to place the I2 cell *before* the fiber, but the restricted space made this option unfeasible. In CHIRON, optical aberrations of the cell may influence the SLSF (sometimes called point spread function or PSF) or shift the spectrum, compared to the non-iodine configuration. This is relevant for

TABLE 2
BASIC OBSERVING MODES OF CHIRON

Mode	Binning H × V	Spectral resolution	Relative efficiency
Slicer	3 × 1	79 000	0.82
Slit	3 × 1	95 000	0.25
Narrow	3 × 1	136 000	0.11
Fiber	4 × 4	27 400	1.0

the stellar template spectra used in forward modeling of the Doppler analysis (see § 3.3). Fortunately, the small beam diameter helps in reducing the aberrations of the cell to an undetectably small level.

After double reflection from the front and back sides of the cell windows, the light interferes with the main (transmitted) parallel beam and modulates the transmitted spectrum with sinusoidal "fringes" that have a relative amplitude of $\sqrt{r_1 r_2}$, where r_1 and r_2 are intensity reflectivity coefficients of the glass surfaces. The fringe period is $\lambda^2/(2dn)$ at wavelength λ for a window of thickness d and refractive index n. Two fringe systems are produced by the two cell windows; very fine fringes resulting from the interference between the windows can usually be neglected.

Fringing is intrinsic to *all* iodine cells. However, under certain conditions (diverging or inclined beam, wedged windows) the modulation is averaged out and becomes acceptably small. This is the case for CHIRON where the cell has 6-mm windows and does not show evidence of fringing. We observed fringing (modulation of the quartz spectra) when other cells with 3-mm windows were placed in CHIRON.

2.4. Mechanical and Thermal Aspects

All optical elements of the spectrograph are mounted on a standard optical table from Thorlabs with a size of $90 \times 75 \times 11$ cm (Fig. 4). The vacuum echelle enclosure and the foreoptics are mechanically attached to the table but extend beyond its perimeter.

The table is oriented horizontally and connected at three points to the steel frame; deformations of the frame should not be transmitted to the optics. An exception is made for the CCD dewar, which is attached to the frame. The dewar

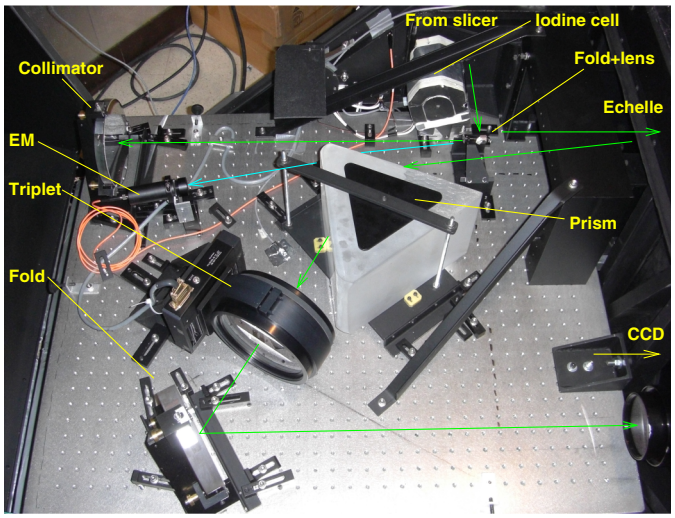

FIG. 4.—Optical elements of CHIRON and the light path. See the electronic edition of the *PASP* for a color version of this figure.

is a source of instability owing to its variable mass and colder temperature; therefore, it is isolated from the main optics mechanically, electrically, and thermally. A light- and air-tight enclosure is integrated with the frame. The enclosure lid can be opened for easy access to the optics. On the outside, the enclosure is covered by thermal insulation (panels of polyisocyanurate foam, thickness 25 mm).

Stabilization of the instrument temperature is important for minimizing displacement of the spectrum on the detector caused by temperature-related mechanical deformations and by the thermal expansion of the grating. As part of the upgrade, CHIRON now has a second stage of insulation. The insulated spectrometer enclosure is surrounded by a "warm room" constructed from an aluminum $80/20$ truss and covered with layers of PRODEX, a lightweight and flexible polyethylene foam covered by aluminum foil on both sides. The thermal room has forced air circulation and air temperature stabilized at $+22$°C by a controlled heater. The temperature was chosen to match the maximum environmental temperature in the Coudé room. This creates a year-round stable environment decoupled from the outside temperature variations. The inner high-precision temperature control of the instrument is done with a 12.5 W internal heater in its support structure, a sensor, and the Lakeshore controller. The set-point is $+23$°C. Owing to good thermal insulation and stable outside air temperature, only a few watts of heating are needed to stabilize CHIRON's internal temperature; low and stable heating power also means small and stable internal temperature gradients. Most of the heat dissipates through the enclosure walls and by conductivity to the dewar, which is not perfectly isolated from the structure. Temperature is monitored at four points inside the instrument. We found that internal temperature variations are five times smaller than the variations of the surrounding air in the thermal room. When thermal control operates normally, the rms fluctuations at all test points are about 0.1°C.

As CHIRON is stationary, the gravity-induced deformation is constant and irrelevant. However, the dispersion direction coincides with the mechanically weak vertical axis of the table. A vertical temperature gradient would bend the table and move the spectrum. We measured a systematic shift of the spectrum with temperature of 1.9 pixel per degree in the dispersion direction and -0.7 pixel per degree in the cross-dispersion direction. In normal operation the spectrum position on the detector is stable to a small fraction of pixel in both directions. Dewar refill shifts the spectrum by 0.07 pixels and that motion is easily tracked by the iodine reference.

A pressure sensor is installed to monitor variations of the atmospheric pressure. This is not as critical since the echelle is now in a vacuum enclosure. The pressure inside the echelle enclosure is also monitored. It grows slowly with time, mostly due to the out-gassing. The enclosure is pumped once the pressure inside it approaches 1% of atmospheric pressure, 8 mB, currently once every five or six months.

CHIRON has two remotely controlled motors, one for focusing (moving the APO-140 triplet mounted on a linear translation stage) and another for moving the slicer unit to change the slit mode. Both motors are manufactured by Physik Instrumente and are driven by the EZSV23 single-board units[8] that connect to the computer by serial lines. The translation of the iodine cell is performed by a simple linear actuator with 50-mm range.

2.5. CCD Detector

The CHIRON detector is a CCD device CCD231-84 from e2v with 4096×4112 square 15 μm pixels. It has a gradient coating in the line direction for optimum sensitivity over a wide spectral range. For this reason we oriented CCD columns parallel to the main (echelle) dispersion, with cross-dispersion along the lines. The CCD is housed in a dewar with liquid nitrogen cooling and a nominal holding time of 36 hr. It is refilled daily during daytime. The CCD temperature is stabilized using a Lakeshore controller.

After CHIRON commissioning in 2011, the detector was operated with a provisional controller which was replaced in 2012 by the new Torrent controller developed at NOAO (Hunten et al. 2010). To our knowledge, CHIRON is the first astronomical instrument to use Torrent. The controller is connected to the dewar by two cables of 40 cm length.

The Torrent controller works with a pixel readout rate of 129 kHz. Readout of the full unbinned chip with all four amplifiers takes ~35 s. We normally use the CCD with 3×1 (binned in the cross-dispersion direction) or 4×4 binning, which shortens the readout time to 18 and 5 s, respectively. The gain is about 1.3 electrons per ADU. The readout noise of 5.4–5.7 electrons in this mode is higher than the intrinsic CCD noise, being affected by a periodic component which shows as a "fringe" pattern in the bias frames and originates in the controller itself.

Linear response of the CCD is important for precise spectroscopy. In this respect, our CCD and controller combination is excellent in the full signal range up to 65 kADU. The ratio of exposure time to counts from a stabilized diffuse light source is constant to 0.5% or better. We developed an alternative method to investigate gain and linearity from the ratio of two images (e.g., quartz lamp spectra). This method does not require flux stability and can be applied to calibration spectra at any time. The charge transfer efficiency is yet another critical parameter for precise RV. It is excellent in both line and column directions; we can only place upper limits on the charge spread of $<10^{-5}$ per transfer.

[8] Please see http://www.allmotion.com for more information.

2.6. Fiber Feed and Guider

The stellar light collected by the telescope is reflected towards the CHIRON fiber by a diagonal pick-off mirror. This mirror is attached to the guide probe inside the regular guiding and acquisition module (GAM) of the 1.5-m telescope. By placing the probe on-axis, we direct the light to CHIRON. The fiber feed (Fig. 5) is permanently available along with the standard on-axis instruments installed at the telescope. The observing time can be shared flexibly between CHIRON and these instruments.

The CHIRON fiber feed module is extremely compact, being restricted by the space available on the side of the GAM. It can be easily detached from the telescope without disconnecting fibers or cables. This is the only way to access the module for alignment and service.

Originally, we used a 15-m fiber with a 100 μm round core (type FPB1001120140 from Polymicro). However, better light scrambling is achieved by a fiber with an octagonal core (Chazelas et al. 2010; Spronck et al. 2012a) and this was installed in 2012 May. This fiber was made by CeramOptec and has a 100 μm octagonal core, 660 μm round cladding, acrylate jacket, length of 20 m, numerical aperture 0.22 ± 0.02, and FC connectors on both ends. The fiber has low focal ratio degradation (FRD), with F/5 input and output at 514 nm the transmission is about 0.87. We found that only $<2 \times 10^{-5}$ of the incoming light is scattered into the fiber cladding (this fiber replaced another octagonal fiber with a silicon-type jacket that resulted in excessive light loss).

In CHIRON, we image the star onto the fiber input end. This is preferable to imaging the telescope pupil because fibers scramble the light spatially (near-field) better than in angle (far field). The far-field (pupil image) is more stable, while the near-field illumination is affected by guiding errors and hence needs better scrambling (see, e.g., Bouchy et al. 2012). The star is re-imaged onto the fiber by two small lenses which transform the beam from $F/7.5$ to $F/5$ (Fig. 5). The 100 μm fiber core projects to 2.7″ on the sky. The fiber is conjugated to the hole of 0.15 mm diameter in the concave and tilted mirror

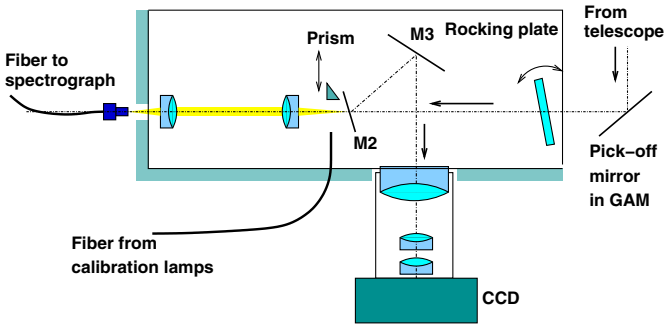

FIG. 5.—Fiber feed of CHIRON. See the electronic edition of the *PASP* for a color version of this figure.

M2 that reflects the surrounding field to the acquisition and guiding camera. Behind the concave mirror, a 2-mm prism can be moved into the beam to direct the light of fiber-coupled comparison lamp into the spectrograph. The prism is driven by a miniature motor HS-85 from Hitek.

The guiding camera contains an uncooled CCD GC 650 from Prosilica with 693×493 pixels, which project at $0.42''$ scale ($3'$ field) on the sky. The guiding is normally done by measuring the centroid of the halo of stellar light around the hole. In the case of binary stars such as α Cen, we can guide on one component while the other is placed in the hole.

Originally, the correction signals were sent to the telescope drives every second. For a fixed exposure time, the average signal on the CCD from the same star varied by a factor of 2 or more. We strongly suspected that poor guiding was the main reason for these variations, as the fiber size of $2.7''$ is large enough to admit most light even under poor seeing. Backlash of the telescope drives, especially in declination, could be the most serious problem affecting the guiding. In 2013 April we installed an improved guiding system to correct the pointing more accurately with a tilted transparent "rocking plate" in front of the focus.

The rocking plate is a 6 mm thick AR-coated window, with a diameter of 40 mm. Its tilt in two orthogonal directions is actuated by two miniature stepper motors.[9] The full range of the plate tilt, $\pm 15°$, provides an image displacement corresponding to $\pm 9.''5$ on the sky. The plate position is currently updated at about 2 Hz. When the plate angles reach a programmable limit, the telescope is commanded to move so that the rocking plate will move back towards the middle of its range. The average gain in the spectrograph throughput was measured over several nights to be 23% after the addition of the tip/tilt module and cleaning of the pick-off mirror.

Calibration lamps, thorium-argon (ThAr) and quartz, are mounted in a separate module and coupled by a fiber with 0.4 mm core to the front-end module. The cathode of the ThAr lamp is imaged onto that fiber by a small lens. A tilted uncoated glass wedge in front of the lens couples the fiber to the quartz lamp (without moving parts). Spatially separated reflections from the wedge allow us to balance the spectrum of the lamp by selective attenuation of its blue and red parts. One side of the wedge projects the quartz lamp directly through the 4-mm thick green filter BG38. Reflection from the other side of the wedge feeds attenuated unfiltered light from the same lamp (mostly red), allowing calibration of orders over the full wavelength range in a single quartz exposure.

2.7. Exposure Meter

An exposure meter was installed as part of the instrument upgrade to calculate a photon-weighted midpoint for the exposure time (Kibrick et al. 2006). This is critical for proper calculation and removal of the barycentric velocity during Doppler planet searches. The exposure meter system at Lick Observatory was originally developed to optimize exposure times for observations with photographic plates. This system uses a reflective propeller blade to divert about 8% of the light from behind the slit to a photo-multiplier tube (Kibrick et al. 2006). The Keck exposure meter has a similar design, including a propeller blade to pick off light behind the slit. At CHIRON, we elected to pick off about 1% of the collimated light before it reaches the grating and direct it to the exposure meter (EM) by an optical fiber. Originally, the 15-mm central part of the beam (which is lost anyway to the central obstruction) was reflected to the EM by a circular mirror with a hole. However, the beam center is "dark" because of the central obstruction in the telescope (the fiber preserves angles, so that the secondary mirror obstruction is imprinted in the outgoing beam). Therefore, during the 2012 upgrade, the circular mirror was replaced by a triangular mirror in front of the vane that supports the small optics near the collimator focus (Fig. 6). The base of the mirror is 5-mm wide, its length is 50 mm. With this repositioned pick-off mirror and larger area, the EM samples about 2% of the collimated beam.

The portion of the parallel beam reflected by the EM mirror is focused by a lens ($D = 50$ mm, $F = 100$ mm) on the SMA fiber with 200-μm core. The fiber delivers light to the photomultiplier model H9319-11 from Hamamatsu. A filter of $545/90$ nm restricts the measured flux to the "iodine" region of the spectrum. The photon counts are accumulated with 0.1 s time cadence and transmitted to the EM computer through a serial interface. A $V = 5^m$ star gives a typical count rate of 10^3 s^{-1} in the EM.

The primary function of the EM is to calculate the flux-weighted midpoint time of exposure, as needed in the precise RV work. However, the EM can also be used to auto-terminate exposures after a given amount of accumulated EM counts are

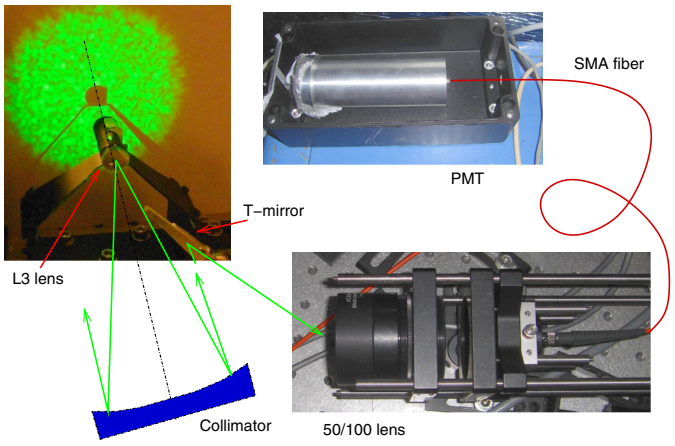

FIG. 6.—Exposure meter. See the electronic edition of the *PASP* for a color version of this figure.

[9] AM1020-2R-V-12-250-23 from http://www.faulhaber.com.

acquired, instead of setting fixed exposure times. This contributes to a more uniform data quality.

2.8. Computers and Software

CHIRON is controlled by three PC computers running under Linux. One is used for taking images, for the instrument control, and for environment monitoring. The CHIRON control software was developed by M. Bonati. All instrument functions (slicer, focus, comparison lamps, iodine cell movements, etc.) are automated. The operator can use a graphical user interface (GUI) for setting instrument parameters and performing exposures. Command-line mode and scripts are also available. The scripting enables automatic calibrations at the beginning and end of the night, setting observing modes by a single command, and interaction with the high-level software (Brewer et al. 2013)

The second computer is responsible for the guiding. It is connected to the GC-650 CCD camera by a reserved Gigabit Ethernet line. The guider software controls the stepper motors and sends commands to the telescope. The third computer serves the exposure meter.

3. OBSERVATIONS AND DATA REDUCTION

3.1. Observing Procedure

The four slit modes of CHIRON and associated CCD binning are listed above in Table 2. We do not change the readout speed of the CCD. Each mode is set by a script. More complex scripts are available to automatically execute sequences of calibration exposures before and after the night. In addition to the slit mode, the operator also must specify the object name, program identifier, and the IN or OUT position of the iodine cell. All these parameters are entered in the GUI.

The telescope is slewed to an object, the star is centered on the fiber using the guiding/acquisition camera, and the guiding loop is closed. At this point, one or several exposures are taken, accompanied if needed by calibration spectra.

Recently, a high-level software for observation planning and execution was implemented to further automate the process (Brewer et al. 2013). The observing program for the night is prepared by the scheduling center at Yale and sent to the local computer at CTIO, where it can be accessed by a browser. The operator selects an object from the target list to observe and the software then sends the target coordinates to the telescope control system, sets up the requested observing mode, and populates all fields in the data-taking GUI. This eliminates potential human errors, leaving to the operator the important tasks of evaluating observing conditions, monitoring the instrument, and reacting to non-standard situations.

After each night, the data are transferred to Yale for quality control and processing. A web-based system for internal data quality check has been developed. In parallel, several parameters are extracted from the CHIRON log files and FITS headers and used to update the web page that displays instrument temperatures, pressure, fluxes, and tracks the resolution and stability from the ThAr spectrum position on the CCD.

3.2. Extraction of Spectra

All CHIRON data are processed at Yale and distributed to other users in both raw and extracted, wavelength-calibrated formats (Fig. 7). Processing is done every morning after observations have been acquired. A text file for each night containing the list of files and their relevant parameters is produced automatically and used to organize the processing.

First, raw images are corrected for bias and gain in each of the four amplifiers to get the combined image in electrons per pixel. The quartz exposures are median-averaged for flat-field (FF) calibration. In the fiber-fed CHIRON, we do not have the possibility to project a wide quartz spectrum for pixel-by-pixel FF correction, as in classical slit spectrographs. Instead, the FF spectrum is normalized by a smoothing polynomial in each order and the flattening calibration is done by dividing the extracted object spectra by the FF spectrum. This method corrects sensitivity variations of the CCD, provided that both star and quartz spectra are extracted from identical pixels. The scattered light between the orders is evaluated and subtracted.

Stability of the order position on the CCD is key to spectrum extraction. The polynomial coefficients describing orders are

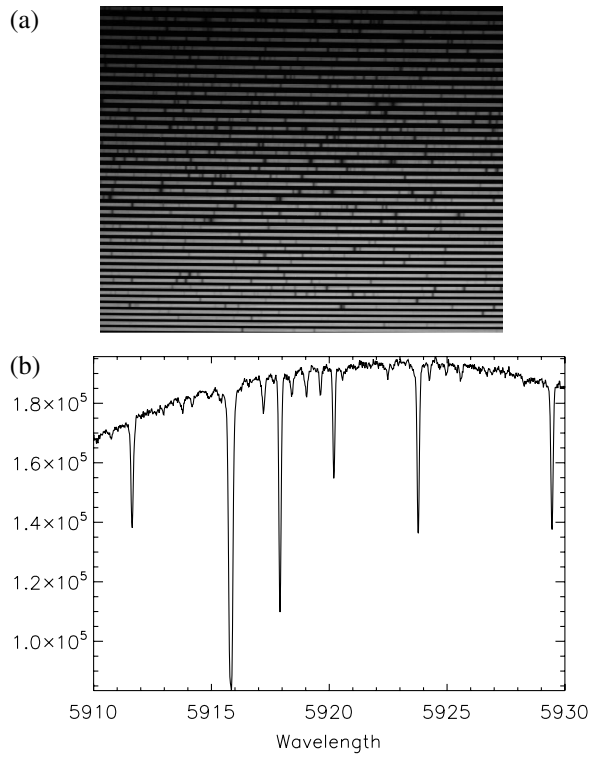

FIG. 7.—*Top*: fragment of the spectrum of a nearby G8V star HD 20794 (82 Eri, $V = 4.26$) in slicer mode recorded on 2011 October 8 with a 10 minute exposure. *Bottom*: portion of the extracted order with S/N of ~400.

defined from the quartz exposures and applied to the stellar spectra. The slit modes differ only by vertical shift and width of the orders, so the same set of order coefficients (refreshed nightly) serves for all modes. This is particularly useful for the slicer mode where the inter-order spacing at long wavelengths is less than the order width. Our standard processing algorithm delivers a set of 62 fixed orders covering the range of 450–885 nm. It discards shorter wavelengths and edges of the orders.

The spectrum extraction algorithm is based on the REDUCE package by Piskunov & Valenti (2002). The spectrum profile across the order is used for removal of cosmic-ray spikes and for optimum spectrum extraction. However, we prefer the boxcar extraction with fixed order width, rather than the optimum extraction. This choice is made to ensure that the flat-field correction uses exactly same pixels with the same (unit) weight. We checked that for faint stars the noise in box-car extraction is insignificantly higher than the noise in optimally extracted spectra.

Wavelength calibration is done by matching nightly extracted spectra of a ThAr lamp to a cataloged list of lines. This is done automatically, using previous solutions as an initial guess. The reduced spectra are written in the FITS files with three dimensional arrays. The first plane of the array contains the wavelength for each pixel and for each order number and is assigned from the nearest (in time) ThAr exposure in the same slit mode. The second plane of the array contains the extracted intensity (in electrons) for each pixel and order.

3.3. Precise RVs with Iodine Reference

The program observations with CHIRON are taken with an iodine cell and we employ a forward modeling technique (Butler et al. 1996) to derive the Doppler shifts. The modeling process requires an intrinsic spectrum of both the target star and the iodine cell. These are multiplied together, with a Doppler shift as a free parameter, and convolved with the SLSF to model our program observations taken with the iodine cell.

The intrinsic spectrum of the iodine cell is obtained by the Fourier Transform Spectrometer (FTS) scan of our iodine cell with $R = 800\,000$ and $\mathrm{S/N} \sim 1000$. To derive the intrinsic spectrum of our target stars, we obtain a one-time set of three or more $R = 136\,000$ template observations taken without the iodine cell and co-add these spectra to clean cosmic rays and to build up the S/N. The coadded template observation must then be deconvolved to yield the intrinsic stellar spectrum that is used in our Doppler analysis. The deconvolution is carried out using a featureless B-star as a light source for the iodine cell; we use a Levenberg-Marquardt algorithm to derive both the iodine wavelength solution and the SLSF that degrades the FTS iodine spectrum to provide a best fit for our B-star iodine observation. This SLSF is adopted for the adjacent template deconvolution to generate the intrinsic stellar spectrum. The B-star iodine observation is also used to assign a wavelength solution to the intrinsic stellar spectrum.

An important advantage of the CHIRON fiber-fed spectrometer is that the SLSF is much less variable than for a slit-fed spectrometer. In tests at Keck HIRES, the SLSF was found to be a factor of ten times more stable with standard circular fibers compared to slit fed spectrometers. Additional tests in the lab show that the SLSF stability is further improved with the use of optical fibers that have an octagonal cross-section (Spronck et al. 2012a). This improved modal scrambling occurs because circular fibers tend to preserve the angle of incidence throughout the wave guide while octagonal fibers break the rotational symmetry. This coupling stability from the fiber is particularly important for the template deconvolution described above and it can also be used to constrain the range of SLSF variability in models of our program observations.

When constructing a Doppler model of wavelength shifts for our program observations, the spectrum is broken into smaller wavelength segments, or "chunks" along the iodine orders. Each chunk is analyzed independently so that the spatially varying SLSF can be modeled over the two dimensional CCD format. For CHIRON, we analyze 760 chunks in 20 orders and each chunk gives a nearly independent measurement of the stellar velocity. The measurement is not entirely independent because we carry out local averaging of the SLSF for neighboring chunks in the last pass of the Doppler code. The standard deviation of the 760 chunk velocities yields the formal measurement uncertainty for each observation. This measurement uncertainty is a function of the S/N. When several observations are taken in a given night, the velocities can be averaged and the nightly error bars will then decrease with the square root of the number of binned observations. The nightly errors are generally smaller than the RV rms scatter over several nights. The RV can change over longer time-lines because of systematic errors in the analysis, instrumental errors, dynamical velocities in the star (e.g., from planetary companions) or from photospheric signals that introduce spectral line asymmetries such as star spots or variability in granulation. We adopt the binned nightly velocity uncertainties as a measure of our instrumental precision and the velocity rms over several nights as a measure of our instrumental stability.

In Figure 8, we show a 12-nights set of RV measurements for the chromospherically inactive star, HD 10700 (τ Ceti), obtained after upgrading CHIRON. The average S/N is 140 in the individual observations. This S/N is controlled by the exposure meter and our Doppler analysis yields single measurement precision of $0.82\ \mathrm{m\,s^{-1}}$. We took six consecutive observations and averaged these velocities to obtain a binned nightly precision of $0.43\ \mathrm{m\,s^{-1}}$. The rms of this 12-nights data set is $0.53\ \mathrm{m\,s^{-1}}$. To the best of our knowledge, this is both the highest precision and RV stability that has been achieved with the iodine Doppler analysis technique.

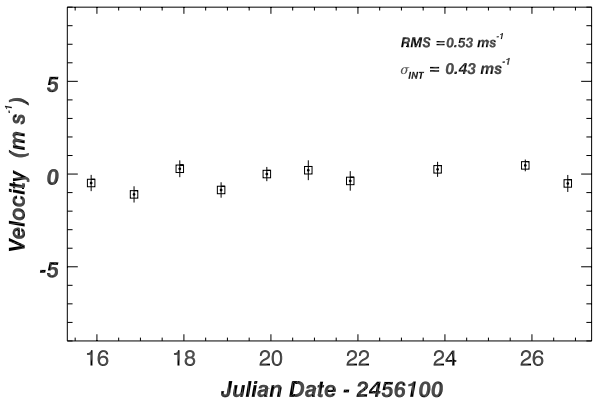

FIG. 8.—Observations of HD 10700 (τ Ceti) taken beginning 2012 July 6 after upgrading CHIRON yield a nightly RV precision of $0.43\ \mathrm{m\,s^{-1}}$, and the rms scatter over 12 nights is $0.53\ \mathrm{m\,s^{-1}}$.

4. CHIRON PERFORMANCE

4.1. Efficiency and Limiting Magnitude

The internal transmission of CHIRON is very high, better than 0.50 in all modes. The octagonal fiber feed is also quite efficient, with transmission of 0.87 at 514 nm (including FRD losses). Considering the known reflectivity of the two telescope mirrors, light loss at the fiber aperture due to seeing, other optics, and the CCD quantum efficiency, we expected the total efficiency at 500 nm (ratio of the photon flux outside the atmosphere to the signal in electrons at blaze peak) to be at least 0.12. Yet, direct measurement with three A-type stars performed on 2012 June 5 (after the upgrade) indicate peak efficiency of only 6%. The measurements repeated on 2013 August 1, using another three standards and reduced by a slightly different method, gave essentially the same result (Fig. 9). We attribute poor efficiency at wavelengths beyond 600 nm to the reduced transmission of the octagonal fiber which was optimized for the iodine region and not characterized at longer wavelengths. The efficiency can still be affected by guiding and/or focusing. Indeed, the flux from α Cen on some nights is at least two times larger than average and agrees well with the expected total efficiency.

Calculation of the signal-to-noise ratio per pixel is based on the following formula:

$$\mathrm{S/N} = N_{\mathrm{ph}}/\sqrt{N_{\mathrm{ph}} + KR^2}, \tag{1}$$

where N_{ph} is the number of stellar photons per spectral pixel collected during the exposure time, $R = 5.5$ is the CCD readout noise in electrons, and K is the number of binned pixels across the order. In the 3×1 slicer mode $K = 9$, the pixel size is about 0.0197 Å at a wavelength of 550 nm. In the fiber mode with 4×4 binning, $K = 2.5$ (assuming optimum extraction) and the spectral pixel is 4 times larger. We calculate N_{ph} by adopting the 6% total efficiency and obtain plots like one in Figure 10. In the regular or narrow slit modes, the efficiency is reduced by additional slit losses. In the fiber mode, the sensitivity is higher and we can reach $\mathrm{S/N} = 20$ on a $V = 12.5^m$ star in a 15-min exposure. Noise in the extracted featureless spectra is indeed in agreement with the above S/N estimates.

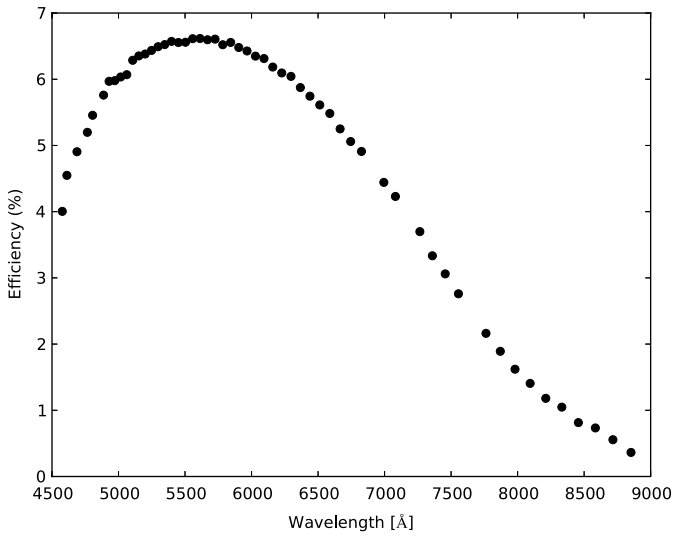

FIG. 9.—Spectral efficiency of CHIRON in fiber mode measured on 2013 August 1 (median for three standard stars, with three exposures of each star). The atmospheric extinction was removed, so that the curve includes only telescope, spectrograph, and detector.

4.2. Stability

The effort to stabilize the instrument resulted in the increased RV precision with iodine calibration (see § 3.3). The RV stability with the standard ThAr wavelength calibration taken immediately before or after program star and cross-correlation of the stellar spectrum was shown to be about 7 $\mathrm{m\,s^{-1}}$ on the 35-day time span (Tokovinin 2013); possibly it can be improved further.

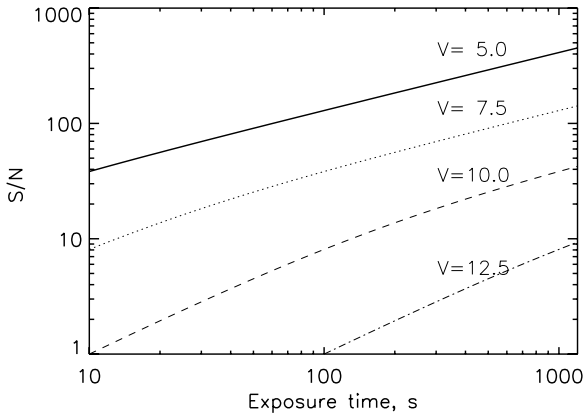

FIG. 10.—S/N per pixel vs. stellar V-band magnitude and exposure time in the slicer mode (at 550 nm near the blaze peak).

TABLE 3
MAIN OPTICAL SURFACE DATA FOR CHIRON

Type	Radius	Thick.	Glass	Diam.	Comment
STD	Inf	15.72	Air	0.1	Fiber exit (Object)
STD	277.83	0.60	SF10	6.25	L1, EO 32301
STD	7.25	2.70	SSKN8	6.25	L1
STD	−7.95	90.0	Air	6.25	L1
STD	Inf	95.06	Air	5	SLICER plane
STD	129.94	2.50	SF5	25.0	L2, EO 32327
STD	44.64	6.00	BK7	25	L2
STD	−61.47	210.0	Air	25	L2
CRB	—	0.00	—	—	TiltX = 45
STD	Inf	0.0	MIRROR	6.25	FOLD 45-deg
CRB	—	−10.0	—	—	TiltX = −45
STD	−8.63	−3.0	BAFN10	6.25	L3, EO 32299
STD	5.29	−0.80	SF10	6.25	L3
STD	51.17	−10.36	Air	6.25	L3
STD	Inf	−609.6	—	—	FOCAL PLANE
STD	1219.2	1083.8	MIRROR	130.0	Limator conic = −1
CRB	—	0.0	—	—	TiltY = 5.5 (gamma)
CRB	—	0.0	—	—	TiltX = −62.74 TiltZ = 90
GRATING	Inf	0.0	MIRROR	265	Echelle 31.6 lpm
CRB	—	0.0	—	—	TiltX = 62.75 TiltZ = −90
CRB	—	−600.0	—	—	TiltY = 5.5 (gamma)
CRB	—	0.0	—	—	TiltX = 54.43
STD	Inf	117.75	LF7	160	PRISM front surface
CRB	—	0.0	—	—	TILTX = −31
STD	Inf	117.75	LF7	160	PRISM mid-plane
CRB	—	0.0	—	—	TILTX = −31
STD	Inf	0.0	Air	160	PRISM back surface
CRB	—	−140.0	—	—	TILTX = 54.34
APO-140	n/a	−57.0	n/a	140	APO-140 triplet
CRB	—	−170	—	—	Distance to fold
CRB	—	0	—	—	TiltX = −29.43
STD	Inf	0	MIRROR	150	FOLD MIRROR
CRB	—	600.7	—	—	TiltX = −29.43
Flattener	n/a	83.0	n/a	86	APO-140 flattener
CRB	—	83.0	—	—	To dewar
STD	Inf	10.0	SILICA	110	Dewar window
STD	Inf	9.0	Air	30	Image plane (CCD)

This opens interesting applications to stars that are too faint for the iodine technique.

4.3. Spectrum Quality

On bright stars, very high S/N can be reached (e.g., $S/N \sim 400$ in Fig. 7). The ultimate limit of the S/N in CHIRON is yet to be established. During CHIRON integration, we used a green laser and were surprised by the lack of parasitic reflections and ghosts: all light went into one location on the CCD. The simplicity of the optical scheme and good coatings contribute to the cleanness of the resulting spectra.

5. SUMMARY

CHIRON is a high resolution (27 000–136 000) facility spectrometer on the 1.5-m telescope at CTIO. The spectrometer was built with supplemental funding to the American Recovery and Reinvestment Act through the NSF MRI program in 2009. The instrument was commissioned in 2011 March and is available to the community through telescope time partnerships with the SMARTS[10] or through the NOAO time allocation committee. Observing is executed by CTIO telescope operators and a data reduction pipeline for supported modes provides extracted spectra for SMARTS observers the day after observations are obtained.

In 2012 January, we carried out several upgrades to improve the throughput and stability of CHIRON for the purpose of improving the precision of RV measurements. The upgrade effort included an exposure meter to calculate the photon-weighted midpoint for observations and to auto-terminate observations at a user-specified S/N, replacement of the echelle grating with

[10] Please see http://www.astro.yale.edu/smarts/ for more information.

one of a higher efficiency, vacuum enclosure for the echelle grating to minimize variability in the dispersion, replacement of the optical fiber feed with an octagonal fiber, AR coating (sol-gel) for optical surfaces, development of a reduction pipeline, program scheduling and quality control software, improved thermal control of the instrument, and a new CCD controller. To assess the impact of these hardware upgrades to CHIRON, we compared our current RV precision for HD 10700 (Fig. 8) with measurements obtained in 2011 (before upgrading CHIRON). This is not a perfect comparison because we cannot control for differences in stellar activity or potential dynamical velocities from planets. However, we see a significant improvement; even with a slightly better average S/N of 155, the typical single-measurement uncertainty before the upgrade was $1.5\ \mathrm{m\,s^{-1}}$ and the lowest rms over any two week stretch in 2011 was $1.91\ \mathrm{m\,s^{-1}}$. Based on this comparison, we conclude that we gained more than a factor of 2 improvement in the single measurement precision. We also controlled systematic errors, improving the instrumental stability, as evidenced by the factor of ~ 4 improvement in the velocity rms over several nights.

To date, four publications that have made use of CHIRON data have appeared in peer-reviewed journals (Tokovinin 2013; Shore et al. 2013; Ingleby et al. 2013; Ratajczak et al. 2013), with additional papers submitted and in preparation. We thank Thomas Blake at the Environmental Molecular Sciences Laboratory (EMSL) for help with FTS scans of the iodine cell. A portion of the research was performed using EMSL, a national scientific user facility sponsored by the Department of Energy's Office of Biological and Environmental Research and located at Pacific Northwest National Laboratory.

The CHIRON was designed and fabricated at the CTIO workshop. DAF acknowledges support for construction of this instrument through the NSF MRI grant 0923441. DAF further acknowledges support for instrument upgrades, software development, and a precision Doppler planet search from Yale University, NSF AST-1109727, and NASA NNS12AC01G. DAF thanks contributors to The Planetary Society for support that advanced our understanding of fiber coupling of spectrographs and provided telescope time.

APPENDIX A.

OPTICAL PRESCRIPTION

Table 3 lists surface data of CHIRON optics, excluding the commercial triplet APO-140 and the wedged window of the echelle enclosure.

REFERENCES

Baranne, A., Queloz, D., Mayor, M., et al. 1996, A&AS, 119, 373
Barden, S. C., & Ingerson, T. E. 1998, in ASP Conf. Ser. 152, Fiber Optics in Astronomy III, ed. S. Arribas, E. Mediavilla, & F. Watson (San Francisco: ASP), 60
Bouchy, F., Diaz, R. F., Hébrard, G., et al. 2012, A&A, 549, 49
Bouchy, F., Pepe, F., & Queloz, D. 2001, A&A, 374, 733
Butler, R. P., Marcy, G. W., Williams, E., et al. 1996, PASP, 108, 500
Brewer, J., Giguere, M., & Fischer, D. A. 2013, PASP, submitted
Chazelas, B., Pepe, F., Wildi, F., et al. 2010, Proc. SPIE, 7739, 134
Crane, J. D., Shectman, S. A., Butler, R. P., et al. 2010, Proc. SPIE, 7735, 170
Fischer, D. A., Gaidos, E., Howard, A. W., et al. 2012, ApJ, 745, 21
Guedes, J. M., Rivera, E. J., Davis, E., et al. 2008, ApJ, 679, 1582
Hearnshaw, J. B., Barnes, S. I., Kershaw, G. M., et al. 2002, Exp. Astron., 13, 59
Hunten, M., Buchholz, N., George, R., et al. 2010, Proc. SPIE, 7742, 53
Ingleby, L., Calvet, N., Herczeg, G., et al. 2013, ApJ, 767, A112
Kibrick, R. I., Clarke, D. A., Deich, W. T. S., & Tucker, D. 2006, Proc SPIE, 6274, 58
Pepe, F., Mayor, M., Delabre, B., et al. 2000, Proc. SPIE, 4008, 582
Perruchot, S., Kohler, D., Bouchy, F., et al. 2008, Proc. SPIE, 7014, 17
Piskunov, N. E., & Valenti, J. A. 2002, A&A, 385, 1095
Raskin, G., Van Winckel, H., Hensberge, H., et al. 2011, A&A, 526, A69
Ratajczak, M., Helminiak, K. G., Konacki, M., & Jordán, A. 2013, MNRAS, 433, 2357
Richardson, N. D., Gies, D. R., & Williams, S. J. 2011, AJ, 142, 201
Schwab, C., Spronck, J. F. P., Tokovinin, A., & Fischer, D. A. 2010, Proc. SPIE, 7735, 149
Schwab, C., Spronck, J., Tokovinin, A., Szymkowiak, A., Giguere, M., & Fisher, D. 2012, Proc. SPIE, 8446, 9
Schroeder, D. J., & Hilliard, R. L. 1980, Appl. Opt., 19, 2833
Shore, S. N., De Gennaro Aquino, I., Schwarz, G. J., et al. 2013, A&A, 553, A123
Spronck, J. F. P., Fischer, D. A., Kaplan, Z. A., Schwab, C., & Szymkowiak, A. E. 2013, PASP, 125, 511
Spronck, J. F. P., Fischer, D. A., Kaplan, Z. A., & Schwab, C. 2012a, Proc. SPIE, 8446, 8ZS
Spronck, J. F. P., Kaplan, Z. A., Fischer, D. A., Schwab, C., & Szymkowiak, A. E. 2012b, Proc. SPIE, 8446, 8TS
Stahl, O., Kaufer, A., & Tubbesing, S. 1999, in ASP Conf. Ser. 188, Optical and Infrared Spectroscopy of Circumstellar Matter, ed. Eike W. Guenther, Bringfried Stecklum, & Sylvio Klose (San Francisco: ASP), 331
Tokovinin, A. 2013, AJ, 145, 76